JCTC Journal of Chemical Theory and Computation
Article
pubs.acs.org/JCTC

Passive Membrane Permeability: Beyond the Standard Solubility-Diffusion Model

Giulia Parisio,*[,‡] Matteo Stocchero,[†] and Alberta Ferrarini[‡]

[‡]Dipartimento di Scienze Chimiche, Università di Padova, Via Marzolo 1, 35131 Padova, Italy
[†]S-IN Soluzioni Informatiche, Via Ferrari 14, 36100 Vicenza, Italy

ABSTRACT: The spontaneous diffusion of solutes through lipid bilayers is still a challenge for theoretical predictions. Since permeation processes remain beyond the capabilities of unbiased molecular dynamics simulations, an alternative strategy is currently adopted to gain insight into their mechanism and time scale. This is based on a monodimensional description of the translocation process only in terms of the position of the solute along the normal to the lipid bilayer, which is formally expressed in the solubility-diffusion model. Actually, a role of orientational and conformational motions has been pointed out, and the use of advanced simulation techniques has been proposed to take into account their effect. Here, we discuss the limitations of the standard solubility-diffusion approach and propose a more general description of membrane translocation as a diffusion process on a free energy surface, which is a function of the translational and rotational degrees of freedom of the molecule. Simple expressions for the permeability coefficient are obtained under suitable conditions. For fast solute reorientation, the classical solubility-diffusion equation is recovered. Under the assumption that well-defined minima can be identified on the free energy landscape, a mechanistic interpretation of the permeability coefficient in terms of all possible permeation paths is given.

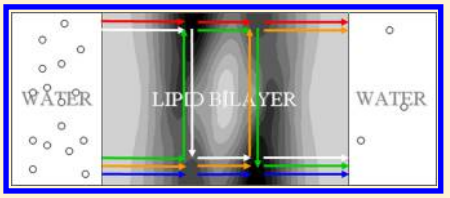

INTRODUCTION

The membrane transport of solutes regulates the cellular uptake and release of substances. Transport processes making use of protein pumps, protein carriers, and channels allow the mediated transport of ions through cell membranes; on the other hand, small solutes and drug-like molecules can permeate the lipid matrix by a diffusion process driven by a concentration gradient between the water regions at the two sides of a bilayer.[1]

The ability of molecular solutes to cross lipid bilayers depends on their chemical structure and is quantified by their *intrinsic permeability coefficient*, P. This is defined from the steady-state flux per unit area across the lipid bilayer, J, and the concentration difference between the bilayer/water interfaces in contact with the donor (D) and acceptor (A) compartments, $C_D - C_A$, according to the relation[2]

$$J = P(C_D - C_A) \tag{1}$$

Experimentally, the concentration difference between bulk solutions at the two membrane sides, which are kept homogeneous by stirring, is measured. Actually, what is determined in this way is the *apparent* permeability coefficient, P_{app}, which may be heavily affected by diffusion through the unstirred water layers between the membrane and the bulk.[3] P_{app} is equal to P for vanishing thickness of the unstirred water layer.

To rationalize the behavior of solutes of different sizes, shapes, and chemical nature, a *solubility-diffusion mechanism* has been proposed.[4] According to this, solutes (*i*) transfer from water to the membrane, (*ii*) diffuse across the membrane, (*iii*) transfer from the membrane to water (Figure 1). If the transfer steps *i* and *iii* are assumed to be so fast that solute partitioning at the membrane/water interfaces is at equilibrium, the solute

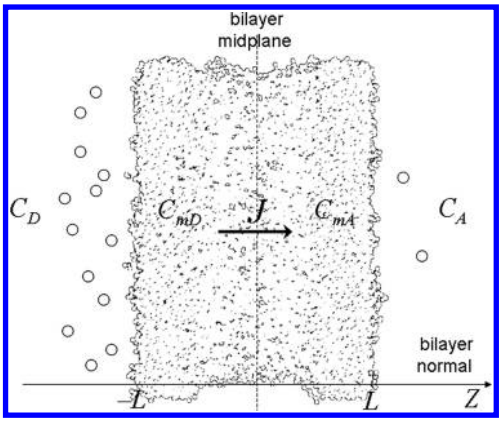

Figure 1. Diffusion across a lipid bilayer: definition of the quantities that enter the solubility-diffusion model.

concentrations (per unit volume) C_{mD} and C_{mA}, just inside the two leaflets of the bilayer, are related to C_D and C_A by the partition coefficient:

$$K = \frac{C_{mD}}{C_D} = \frac{C_{mA}}{C_A} \tag{2}$$

If the lipid bilayer is treated as a homogeneous oil slab, the first Fick's law

$$J = D\frac{C_{mD} - C_{mA}}{2L} = D\frac{K(C_D - C_A)}{2L} \tag{3}$$

Received: August 2, 2013
Published: October 16, 2013

   dx.doi.org/10.1021/ct400690t | *J. Chem. Theory Comput.* 2013, 9, 5236−5246

can be used to derive a simple expression for the permeability coefficient P of the solute in terms of its membrane/water partition coefficient K, its membrane diffusion coefficient D, and the membrane thickness $2L$:

$$P = \frac{DK}{2L} \tag{4}$$

According to this equation, the translocation through a membrane is faster for a lipophilic solute ($K > 1$) than for a hydrophilic one ($K < 1$) having the same diffusion coefficient.

Equation 4 has the valuable feature of conjugating the effects of partition and diffusion properties, whose fundamental role, as determinants of solute permeability, has been widely recognized. The correlation between the permeability of solutes and their oil/water partition coefficient was stated in the late 19th century by Ernest Overton in his famous rule.[5,6] The *n*-octanol/water partition coefficient of a compound, proposed on this basis as a good indicator of its membrane permeability, is still commonly used to this purpose.[7] A critical role of the molecular weight of solutes was also recognized, which was ascribed to the size-dependence of their diffusion coefficients.[8] This was found to be much steeper than in most liquid hydrocarbons and did not comply with the Stokes−Einstein hydrodynamical model, especially in the case of small molecules such as water or urea. The selectivity of biological membranes and lipid bilayers for permeant size was found to be similar to that of polymer membranes.[9,10] According to the "soft-polymer" theory, the solute diffusion would proceed through adjacent transient cavities produced by molecular fluctuations in the membrane and would be governed by the frequency of cavity formation and by the cavity size distribution.[9,10]

The drastic approximation intrinsic to eq 4 is the representation of the lipid bilayer as a homogeneous hydrocarbon layer, where solute partition and diffusion coefficients are uniform. Actually, the bilayer environment is highly heterogeneous along the direction normal to the membrane surface, and the permeability of a solute is determined by its difficulty to cross a confined region, characterized by the most unfavored partitioning and/or the slowest diffusion. For hydrophilic solutes, this region has been identified with the hydrocarbon domain of the bilayer, and alkane solvents like hexadecane, or more polarizable alkene solvents, have been taken to mimic this microenvironment.[11,12] However, the anisotropic packing of lipids differentiates the ordered bilayer environment from isotropic bulk solvents, and the influence of chain ordering on both solute partitioning and diffusion has been proposed to explain the size selectivity of transport across lipid bilayers.[13,14] Furthermore, it has been proven experimentally that solute uptake depends also on the membrane surface density.[15] To account for the independent contributions of the headgroup and tail regions to the overall resistance to permeation, a three layer theory based on a modified solubility-diffusion approach was recently presented, where both the area per lipid and the thickness of the hydrocarbon core appear as structural parameters in the expression for the permeability coefficient.[16]

An *inhomogeneous solubility-diffusion model* was proposed to provide a more realistic description of membrane transport;[17] subsequently, a molecular dynamics (MD) simulation-based methodology, for the calculation of nonuniform partition and diffusion coefficients through lipid bilayers was developed.[18] This represents now the standard computational approach for the evaluation of membrane permeability coefficients.[19]

In this paper, we address the theoretical description of solute permeation through lipid membranes in more general terms and show how simple expressions for the permeability coefficient can be derived under suitable conditions. In the next sections, the classical solubility-diffusion model will be outlined in connection with MD simulations. Intrinsic to this approach is the reduction of permeation to an effective translational process, where any degree of freedom other than the position of the permeant molecule along the bilayer normal is assumed to be irrelevant. The model will be then recast in the general framework of a multidimensional Fokker−Planck equation, and the classical solubility-diffusion expression for permeability will be recovered as a particular case, when the translation of the solute across the bilayer determines the permeation rate. A solution of the roto-translational problem based on a discrete description of the transmembrane diffusion process will be presented.[20] This leads to an expression for the permeability coefficient in terms of the rates for the transitions along all the possible translocation paths, which will be rationalized according to the discrete path sampling theory.[21] Application to selected systems will allow us to illustrate this methodology and to compare the multidimensional approach with the classical monodimensional approximation. Finally, the conclusions of this work will be summarized.

THEORY

The Classical Inhomogeneous Solubility-Diffusion Model: Uses and Limitations. The inhomogeneous solubility-diffusion model was proposed in 1974 by Diamond et al.[17] Under the assumption that diffusion in the membrane interior can be described by the Nernst−Planck equation, and in the absence of activated processes causing abrupt changes in solute chemical potential or mobility at the water/membrane interfaces, the following expression for the steady-state flux of solute molecules through the membrane was obtained:[17]

$$J = -\frac{C(L) - C(-L)}{\int_{-L}^{L} \frac{1}{K(Z)\,D(Z)}\,\mathrm{d}Z} \tag{5}$$

where K and D are the local partition and diffusion coefficient, respectively, which depend on the solute position Z along the bilayer normal. The integration limits ($\pm L$) represent the boundaries of the bilayer (a symmetric bilayer is assumed, as in Figure 1). Thus, the intrinsic permeability coefficient P of the solute is given by

$$\frac{1}{P} = \int_{-L}^{L} \frac{1}{K(Z)\,D(Z)}\,\mathrm{d}Z \tag{6}$$

The function under the integral in eqs 5 and 6 represents the local resistance opposed by the membrane to solute permeation: high affinity for the bilayer environment and/or high diffusion rate yield low resistance and thus high solute permeability. In this way, the permeability of a solute turns out to be determined by the crossing of the so-called *barrier region*, i.e., the region within the bilayer that opposes the highest resistance to solute permeation.[17] Neither $K(Z)$ nor $D(Z)$ are experimentally accessible quantities, and Diamond and Katz could only draw the expected qualitative form of the $D(Z)$ and $K(Z)$ profiles of nonelectrolytes.[17] $K(Z)$, in particular, was assumed to be lower than 1 for hydrophobic and higher than 1 for hydrophilic compounds through the whole bilayer thickness, taking bulk water as a reference. Since D is not expected to vary by orders of magnitude, its effect on the resistance profile will be minor, compared to that of K. Under this assumption, the membrane actually represents a barrier to the passage of a hydrophilic specie

but not for a hydrophobic one, which is transported faster through the bilayer than in water.

Equation 5 has the same form of the expression obtained in 1940 by Kramers for the stationary diffusive flux of particles subject to Brownian forces and to a potential field, $U(Z)$, in the large friction limit, if $K(Z) = \exp[U(Z)/k_BT]$.[22] For the case of a single, smooth potential barrier, large compared to k_BT, Kramers proposed an approximate form of the integral in eqs 5 and 6, which yields

$$P = D_{max}\sqrt{\frac{|\ddot{U}_{max}|}{2\pi k_BT}}\ \exp\left[-\frac{U_{max}}{k_BT}\right] \quad (7)$$

where U_{max} is the height of the barrier, and both the potential curvature, $\ddot{U}_{max}$, and the diffusion coefficient, D_{max}, are evaluated on the top of the barrier. This connection with the Kramers theory has been generally disregarded in the literature, with only very few exceptions.[23] Recently, a relation between the height of the energy barrier and the permeability coefficient was pointed out, and an empirical dependence on the inverse of the barrier height was suggested.[24] Of course, the approximate eq 7 can be appropriate only in the case of hydrophilic permeants showing a single high energy barrier (low K) in the apolar region around the center of the bilayer.

Equation 6 holds for an arbitrarily shaped resistance profile, and for hydrophobic solutes that favorably partition throughout the membrane (large K), it predicts high permeabilities. The physical meaning of this was questioned, based on the consideration that deep free energy minima should act as traps for the solutes inside the bilayer, so lowering their permeability.[24] However, it is important to realize that under steady state conditions, for which eq 6 is derived, free energy minima rather serve as basins where the hydrophobic solutes accumulate, so feeding the outward flux, which results in high permeability. It is worth noticing that the sensitivity of the permeability coefficient to partition properties inside the bilayer is larger for hydrophilic than for hydrophobic species: the rising of the energy barrier for a hydrophilic compound causes a rapid decrease of P; the increase of P caused by the deepening of the energy well for a hydrophobic solute is slower, and for deep enough energy minima, P tends to a constant value. This can be understood considering the shape of the $K(Z)$ profile for a hydrophobic solute: the well region within the bilayer, where $K \gg 1$, gives a negligible contribution to the integral in eq 6 compared to the side regions where K raises to 1 at the water/bilayer interfaces. The negligible dependence of P on the depth of the energy well for hydrophobic solutes was derived also in ref 16 by a different approach.

Direct observation of a significant number of successful permeation events by standard atomistic MD simulations, although possible in principle, requires prohibitively long trajectories. Coarse-grained representations of the lipid environment allow one to reduce the computational cost; however, the number of long enough trajectories that can be sampled in a computationally feasible time remains statistically inadequate. In 1994, Marrink and Berendsen[18] proposed a computational method based on the inhomogeneous solubility-diffusion model (eq 6), which became the standard approach for the calculation of permeability coefficients.[25−27] MD simulations with solute particles constrained at different positions Z across a lipid bilayer are performed, and the profiles of the partition and diffusion coefficients, $K(Z)$ and $D(Z)$ in eq 6, are computed from the average value of the constraint force and from the autocorrelation function of its fluctuation, respectively.[18]

Although the inhomogeneous solubility-diffusion model represents a state-of-the-art approach in the computational investigation of membrane permeation,[28,29] it has an important limitation in that it considers a single reaction coordinate corresponding to the position of the solute along the bilayer normal. The underlying assumption is that this is the only slow degree of freedom, i.e., that only solute translation through the bilayer determines the transmembrane transport rate. In principle, a single reaction coordinate could be used to describe the translocation progress;[30] however, its identification is not straightforward. The position along the bilayer normal, Z, represents the intuitive choice, but it may not coincide, in general, with the intrinsic reaction coordinate, which contains the slow variables determining the rate of the permeation process.[31] Actually, the importance of orientational and conformational motions, especially in the case of large permeants, was recently pointed out, and the use of advanced simulation techniques was proposed for the study of unassisted solute permeation through lipid bilayers. In ref 32, milestoning was proposed as a suitable choice, since its theory and algorithm, based on the sampling of short trajectories, are not restricted to one-dimensional (1D) dynamics. However, in that work, the method was applied only for a 1D description of the permeation of a blocked tryptophan through a DOPC bilayer. Ghaemi et al. used bias-exchange metadynamics for the enhanced sampling of the free energy surface for ethanol in a POPC bilayer; based on this, they defined a kinetic model and then performed a long kinetic Monte Carlo simulation to estimate the permeability coefficient of ethanol.[33] More recently, Jämbeck and Lyubartsev employed multiple walkers metadynamics in conjunction with well-tempered metadynamics to obtain the free energy surfaces of aspirin, diclofenac, and ibuprofen in a DOPC bilayer, as a function of their distance from the bilayer center and of selected conformational degrees of freedom.[34] In this way, they were able to discuss the role of the conformational variables on partitioning and on permeation rate.

For relatively large molecules, reorientations can take place on the same time scale of displacements along the bilayer normal, so the coupling between positional and orientational degrees of freedom could be particularly important. Spontaneous flip-flop is probably the most outstanding example of roto-translational diffusion: it not only represents a mechanism for the interleaflet transfer of membrane components like phospholipids and sterols but also occurs during the transmembrane translocation of permeants like amphiphilic drugs and fatty acids.[35−37] In a recent study of steroid flip-flop, we took into account the energetic and frictional coupling between molecular rotation and translation, within a kinetic description based on the analysis of the free energy surface of the steroids in the bilayer environment. The results clearly demonstrated that reorientational motions can be slow enough to limit the rate of the transport of solutes across the bilayer.[20]

While taking into account the nonuniformity of the membrane environment, the inhomogeneous solubility-diffusion model does not include roto-translational coupling effects. These are necessarily introduced by the anisotropy and order of the lipid bilayer but cannot be revealed by MD simulations when the constrained particle method is adopted. Indeed, during constrained simulations, solute particles explore different orientations, and hence, provided that an efficient statistical sampling is performed, orientational effects on K and D are averaged out. Despite this, the inhomogeneous solubility-diffusion model and the standard MD methodology for the computation of the permeability coefficient are commonly adopted without restriction,[23,24] even when relevant orientational changes in the insertion path of a solute are hypothesized.[38]

The Stochastic Description of Permeation As Roto-Translational Diffusion. At equilibrium, the distribution of a solute is only determined by solute-membrane interactions therefore, in a symmetric bilayer, it is symmetrical with respect to the bilayer midplane. A concentration gradient induces an imbalance in solute concentration between the two leaflets of the bilayer and hence a nonequilibrium distribution of the solute, driving the diffusion of the solute across the membrane: the permeating flux is established to take the system to equilibrium. In the heterogeneous and anisotropic membrane environment, the coupling between the positional (X,Y,Z) and orientational (α,β,γ)[39] variables, which is integral to the potential field experienced by the solute, causes the evolution of the system by roto-translational diffusion. Actually, given the axial symmetry of the bilayer environment, only the Z coordinate and the $\Omega = (\beta,\gamma)$ Euler angles need to be specified: β is the polar angle between the bilayer normal and the z axis of the molecular frame defined on the solute; the azimuthal angle γ specifies the rotation around this axis.

The diffusion equation

$$\frac{\partial}{\partial t}C(\Omega, Z, t) = -\vec{\nabla}^T\vec{J}(\Omega, Z, t) \tag{8}$$

governs the time evolution of the nonequilibrium concentration field $C(\Omega,Z,t)$. The flux vector $\vec{J}(\Omega,Z,t)$ has translational and rotational components, which are independent under the assumption of negligible dynamic roto-translational coupling

$$\vec{J}(\Omega, Z, t) = \begin{pmatrix} \vec{J}_{\text{transl}}(\Omega, Z, t) \\ \vec{J}_{\text{rot}}(\Omega, Z, t) \end{pmatrix}; \vec{J}_{\text{transl}} = \begin{pmatrix} J_X \\ J_Y \\ J_Z \end{pmatrix} \vec{J}_{\text{rot}} = \begin{pmatrix} J_\alpha \\ J_\beta \\ J_\gamma \end{pmatrix} \tag{9}$$

Since the permeability coefficient is related only to the component of the flux along the bilayer normal, J_Z, eq 8 is conveniently rewritten in the form

$$\frac{\partial}{\partial t}C(\Omega, Z, t) = -\frac{\partial}{\partial Z}J_Z(\Omega, Z, t) + \ldots \tag{10}$$

where the dots stand for all the terms that do not contribute and, hence, in the following will not be shown explicitly.

Within a stochastic theoretical framework, the Fokker–Planck–Smoluchowski equation[40,41]

$$\frac{\partial}{\partial t}p(\Omega, Z, t) = \Gamma(\Omega, Z)\, p(\Omega, Z, t) \tag{11}$$

describes the time evolution of the nonequilibrium distribution function $p(\Omega,Z,t)$ in terms of the roto-translational diffusion operator Γ, defined as

$$\Gamma(\Omega, Z) = \vec{\nabla}^T\mathbf{D}(\Omega, Z)\, p_{\text{eq}}(\Omega, Z)\vec{\nabla}\, p_{\text{eq}}^{-1}(\Omega, Z) \tag{12}$$

Here, $p_{\text{eq}}(\Omega,Z)$ is the equilibrium distribution function which represents the thermodynamic limit of the evolution of $p(\Omega,Z,t)$:

$$\lim_{t\to+\infty} p(\Omega, Z, t) = p_{\text{eq}}(\Omega, Z) \tag{13}$$

and both $p(\Omega,Z,t)$ and $p_{\text{eq}}(\Omega,Z)$ are defined to satisfy the normalization conditions

$$\int_{-L}^{L} \mathrm{d}Z \int p(\Omega, Z, t)\, \mathrm{d}\Omega = \int_{-L}^{L} \mathrm{d}Z \int p_{\text{eq}}(\Omega, Z)\, \mathrm{d}\Omega = 1 \tag{14}$$

where the integration limits $(\pm L)$ represent symmetric bilayer boundaries.

The equilibrium distribution function is related to the roto-translational potential field $U(\Omega,Z)$ by

$$p_{\text{eq}}(\Omega, Z) = \frac{\exp\left[-\frac{U(\Omega, Z)}{k_{\text{B}}T}\right]}{\int_{-L}^{L} \mathrm{d}Z \int \mathrm{e}^{-U(\Omega,Z)/k_{\text{B}}T}\, \mathrm{d}\Omega} \tag{15}$$

Both the $\vec{\nabla}$ operator (the superscript T indicates the transpose) and the diffusion tensor $\mathbf{D}$ in eq 12 have translational and rotational components, which can be expressed in terms of the positional and orientational variables, respectively (see Appendix A). In the absence of dynamic roto-translational coupling, the diffusion operator Γ can be written as

$$\Gamma(\Omega, Z) = \Gamma_{\text{transl}}(\Omega, Z) + \Gamma_{\text{rot}}(\Omega, Z) \tag{16}$$

so that the evolution of the nonequilibrium distribution $p(\Omega,Z,t)$ is described by the two independent operators:

$$\Gamma_{\text{transl}}(\Omega, Z) = \vec{\nabla}_{\text{transl}}^T\mathbf{D}_{\text{transl}}(\Omega, Z)\, p_{\text{eq}}(\Omega, Z)\vec{\nabla}_{\text{transl}}\, p_{\text{eq}}^{-1}(\Omega, Z) \tag{17a}$$

$$\Gamma_{\text{rot}}(\Omega, Z) = \vec{\nabla}_{\text{rot}}^T\mathbf{D}_{\text{rot}}(\Omega, Z)\, p_{\text{eq}}(\Omega, Z)\vec{\nabla}_{\text{rot}}\, p_{\text{eq}}^{-1}(\Omega, Z) \tag{17b}$$

From the analogy between the descriptions based on eqs 8 and 11, the normal component of the flux at depth Z due to solute particles in the orientation Ω can be expressed as

$$J_Z(\Omega, Z, t) = -D_{ZZ}(\Omega, Z)\, p_{\text{eq}}(\Omega, Z)\, \frac{\partial}{\partial Z}p_{\text{eq}}^{-1}(\Omega, Z)\, C(\Omega, Z, t) \tag{18}$$

The total flux of permeant J in eq 1 arises from the diffusion of solute particles in all possible orientations

$$J(Z, t) = \int J_Z(\Omega, Z, t)\, \mathrm{d}\Omega \tag{19}$$

that, under the steady-state condition,

$$\frac{\partial}{\partial t}C(\Omega, Z, t) = 0 \tag{20}$$

must be both constant in time and uniform in space:

$$\frac{\partial}{\partial t}C(\Omega, Z, t) = \frac{\partial}{\partial t}\int C(\Omega, Z, t)\, \mathrm{d}\Omega = \frac{\partial}{\partial Z}\int J_Z(\Omega, Z, t)\, \mathrm{d}\Omega = \frac{\partial}{\partial Z}J(Z, t) = 0 \tag{21}$$

$$J(Z, t) = J \tag{22}$$

Once the time-dependence is dropped from eq 18, a general expression is obtained for the flux:

$$J = -\int D_{ZZ}(\Omega, Z)\, p_{\text{eq}}(\Omega, Z)\, \frac{\partial}{\partial Z}p_{\text{eq}}^{-1}(\Omega, Z)\, C(\Omega, Z)\, \mathrm{d}\Omega \tag{23}$$

At this stage, it is useful to introduce a separation of variables and to rewrite the nonequilibrium probability distribution as the product

$$p(\Omega, Z) = p^{\Omega}(Z)\, p(\Omega; Z) \tag{24}$$

between the conditional probability, $p(\Omega;Z)$, that a solute particle in Z is found in the orientation Ω, and the orientationally averaged positional distribution

dx.doi.org/10.1021/ct400690t | J. Chem. Theory Comput. 2013, 9, 5236−5246

$$p^{\Omega}(Z) = \int p(\Omega, Z)\, d\Omega \tag{25}$$

which are defined so that the normalization conditions

$$\int_{-L}^{L} p^{\Omega}(Z)\, dZ = \int p(\Omega; Z)\, d\Omega = 1 \tag{26}$$

hold. Correspondingly, the nonequilibrium concentration field is given by

$$C(\Omega, Z) = C^{\Omega}(Z)\, p(\Omega; Z) \tag{27}$$

where

$$C^{\Omega}(Z) = \int C(\Omega, Z)\, d\Omega \tag{28}$$

After some algebraic manipulation, eq 23 can be rewritten as

$$J = p_{eq}^{\Omega}(Z)\left\{\frac{\partial}{\partial Z}\left[\left(\frac{C^{\Omega}(Z)}{p_{eq}^{\Omega}(Z)}\frac{p(\Omega; Z)}{p_{eq}(\Omega; Z)}\right)\left(\frac{p_{eq}(\Omega; Z)}{p(\Omega; Z)}D_{ZZ}^{\Omega}(Z) - D_{ZZeq}^{\Omega}(Z)\right)\right] + \frac{\partial}{\partial Z}\left[\frac{C^{\Omega}(Z)}{p_{eq}^{\Omega}(Z)}\frac{p(\Omega; Z)}{p_{eq}(\Omega; Z)}\right]D_{ZZeq}^{\Omega}(Z)\right\} \tag{29}$$

where the orientational averages of the diffusion coefficient in either steady-state or equilibrium conditions appear:

$$D_{ZZ}^{\Omega}(Z) = \int D_{ZZ}(\Omega, Z)\, p(\Omega; Z)\, d\Omega \tag{30a}$$

$$D_{ZZeq}^{\Omega}(Z) = \int D_{ZZ}(\Omega, Z)\, p_{eq}(\Omega; Z)\, d\Omega \tag{30b}$$

Compared to eq 5, eq 29 represents a general expression for the flux J of the solute as a function of both rotational and translational degrees of freedom. To extract the expression for the permeability coefficient P, eq 29 should now be reduced in a form where J is proportional to the concentration difference between the bilayer/water interfaces. An analytical expression for P is easily derived under suitable conditions.

An Expression for the Permeability Coefficient. *Fast Rotational Motions.* When a time scale separation is assumed between the reorientational and translational dynamics, such that the former is much faster than the latter, the orientational distribution at any position can be assumed to be at equilibrium, so that

$$p(\Omega; Z) = p_{eq}(\Omega; Z) \tag{31}$$

and

$$D_{ZZ}^{\Omega} = D_{ZZeq}^{\Omega} \tag{32}$$

Substituting eqs 31 and 32 into eq 29 and rearranging gives

$$\frac{J}{p_{eq}^{\Omega}(Z)\, D_{ZZeq}^{\Omega}(Z)} = \frac{\partial}{\partial Z}\left[\frac{C^{\Omega}(Z)}{p_{eq}^{\Omega}(Z)}\right] \tag{33}$$

After integration on Z over the bilayer thickness, eq 33 yields

$$J = \frac{C^{\Omega}(L) - C^{\Omega}(-L)}{p_{eq}^{\Omega}(L)\int_{-L}^{L}\frac{1}{p_{eq}^{\Omega}(Z)D_{ZZeq}^{\Omega}(Z)}\, dZ} \tag{34}$$

where the local membrane/water partition coefficient, averaged over all orientations, can be recognized in the ratio

$$K_{eq}^{\Omega}(Z) = \frac{p_{eq}^{\Omega}(Z)}{p_{eq}^{\Omega}(L)} \tag{35}$$

The main equation of the heterogeneous solubility-diffusion model is then recovered

$$\frac{1}{P} = \int_{-L}^{L}\frac{1}{K_{eq}^{\Omega}(Z)D_{ZZeq}^{\Omega}(Z)}\, dZ \tag{36}$$

if the position-dependent partition and diffusion coefficients K and D in eq 6 are identified with the corresponding quantities, defined as orientational averages, K_{eq}^{Ω} and D_{ZZeq}^{Ω} in eq 36.

Discrete Stable States. In the presence of high barriers between the minima of the $U(\Omega,Z)$ surface, fast librations in the potential wells can be disregarded, and the permeation process can be described by a kinetic model.[43] One can picture the permeant molecules to first leave the donor compartment on one side of the membrane, visit a number of stable sites within the bilayer, corresponding to energy minima, and finally reach the acceptor compartment on the other side. The time evolution of the system is described in terms of the transitions between these discrete states, according to the master equation[44]

$$\frac{\partial}{\partial t}p_j(t) = -\sum_{j'} W_{jj'}p_{j'}(t) \tag{37}$$

where p_j is the discrete analogue of the probability distribution in eq 11 for the j state, $W_{jj'}$ for $j \neq j'$ is the opposite of the rate of the $j' \rightarrow j$ transition

$$k_{j\leftarrow j'} = -W_{jj'} \tag{38}$$

and

$$W_{jj} = \sum_{q} k_{q\leftarrow j} \tag{39}$$

Under these conditions, in the presence of the potential field $U(\Omega,Z)$, the equilibrium probability distribution can be approximated by the discrete probabilities of configurations corresponding to the energy minima

$$p_{jeq} = \frac{\exp[-E_j/k_BT]}{\sum_m \exp[-E_m/k_BT]} \tag{40}$$

with

$$E_j = U_j + \frac{k_BT}{2}\ln\left|\det\frac{\ddot{\mathbf{U}}_j}{2\pi k_BT}\right| \tag{41}$$

where U_j and $\ddot{\mathbf{U}}_j$ are the value of potential and the matrix of its second derivatives, respectively, both calculated in the minimum j. The Kramers approximation generalized to diffusion on a multidimensional potential surface[43,45] gives the rate of a transition connecting the free energy minima j' and j through the saddle point s

$$k_{j\leftarrow j'} = -\frac{\lambda_s}{2\pi k_BT}\sqrt{\frac{|\det \ddot{\mathbf{U}}_{j'}|}{|\det \ddot{\mathbf{U}}_s|}}\exp\left[-\frac{(U_s - U_{j'})}{k_BT}\right] \tag{42}$$

where λ_s is the single negative eigenvalue of the product matrix $\mathbf{D}\ddot{\mathbf{U}}$, between the roto-translational diffusion tensor $\mathbf{D}$ and the curvature matrix $\ddot{\mathbf{U}}$, both calculated at the saddle point.

dx.doi.org/10.1021/ct400690t | J. Chem. Theory Comput. 2013, 9, 5236−5246

Under steady-state conditions in the presence of a flux J per unit area, the time evolution of the probability in the donor (D) and acceptor (A) basins and in each intermediate state (I) in the bilayer is given by

$$\frac{\partial p_{\mathrm{D}}(t)}{\partial t} = -\frac{\partial p_{\mathrm{A}}(t)}{\partial t} = -Ja$$
$$\frac{\partial p_{\mathrm{I}}(t)}{\partial t} = 0 \tag{43}$$

where a is the bilayer surface area.

If N_{I} is the number of stable configurations in the membrane, eqs 37 and 43 give a linear system of $N_{\mathrm{I}} + 1$ independent equations in $N_{\mathrm{I}} + 2$ unknown probabilities. With the additional constraint of the normalization condition

$$p_{\mathrm{D}} + \sum_{I=1}^{N_{\mathrm{I}}} p_{\mathrm{I}} + p_{\mathrm{A}} = 1 \tag{44}$$

the solution of the system yields the discrete probabilities p_i and, by definition (eq 1), the permeability coefficient

$$P = \frac{Ja}{\left(\frac{p_{\mathrm{D}}}{l_{\mathrm{D}}} - \frac{p_{\mathrm{A}}}{l_{\mathrm{A}}}\right)} \tag{45}$$

where $l_{\mathrm{D/A}}$ is the extent of the D/A basin along the direction of the bilayer normal.

The complexity of the resulting expression for P in terms of the rates of all the transitions connecting the states in the system grows as the number of states and their connectivity increase, but can be rationalized in the framework of Discrete Path Sampling (DPS) theory,[21] as explained in the following.

Calculating the Permeability Coefficient from the Transition Rate Constants. The kinetic approach outlined in the last section (eqs 37 and 43) is equivalent to describing the system in terms of the effective two-state dynamics between the donor and acceptor basins:

$$\frac{\partial p_{\mathrm{D}}(t)}{\partial t} = -k_{\mathrm{A}\leftarrow\mathrm{D}}\, p_{\mathrm{D}}(t) + k_{\mathrm{D}\leftarrow\mathrm{A}}\, p_{\mathrm{A}}(t)$$
$$\frac{\partial p_{\mathrm{A}}(t)}{\partial t} = k_{\mathrm{A}\leftarrow\mathrm{D}}\, p_{\mathrm{D}}(t) - k_{\mathrm{D}\leftarrow\mathrm{A}}\, p_{\mathrm{A}}(t) \tag{46}$$

where the effective rate constants $k_{\mathrm{A}\leftarrow\mathrm{D}}$ and $k_{\mathrm{D}\leftarrow\mathrm{A}}$, which are equal in a symmetric system, are related to the permeability coefficient by

$$P = k_{\mathrm{A}\leftarrow\mathrm{D}} l_{\mathrm{D}} = k_{\mathrm{D}\leftarrow\mathrm{A}} l_{\mathrm{A}} \tag{47}$$

DPS theory provides a neat form for the effective rate constants arising from the contributions of all possible pathways connecting the two states D and A.[21] Given the equalities in eq 47, we choose to refer, from now on, to the D → A process.

There is an infinite number of paths connecting D to A through the intermediate states I, which includes paths involving recrossings (successive forward and backward transitions between a pair of states) and cycles (transition sequences leading to multiple passages through a single state), and all of these paths contribute to the effective rate constants. Each path starts with a transition from the donor basin to any intermediate state connected to it, D → i, and ends with a transition from any intermediate state connected to the acceptor basin to the latter, f → A. Paths going through the same i and f states can connect them with a number of steps s ranging from 1 to infinite (Figure 2).

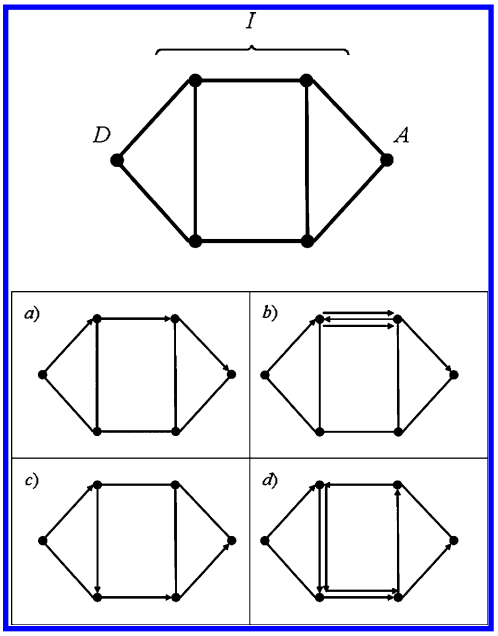

Figure 2. Representation of a possible connection scheme between donor (D), acceptor (A), and intermediate (I) states, and possible pathways going from D to A either directly (a and c) or through recrossings (b) and cycles (d).

Each transition $j \rightarrow j'$, from an intermediate state j, gives a contribution to $k_{\mathrm{A}\leftarrow\mathrm{D}}$ equal to[21]

$$\frac{k_{j'\leftarrow j}}{\sum_q k_{q\leftarrow j}} \tag{48}$$

where the summation runs over the states and basins connected to the j state.

If the $N_{\mathrm{I}} \times N_{\mathrm{I}}$ weighted adjacency matrix $\mathbf{A}$ between intermediate states is introduced, with elements[21]

$$[\mathbf{A}]_{jj'} = \begin{cases} \dfrac{k_{j'\leftarrow j}}{\sum_q k_{q\leftarrow j}}, & \text{for } j \text{ and } j' \text{ connected} \\ 0, & \text{otherwise} \end{cases} \tag{49}$$

the if element of the $\mathbf{A}^s$ matrix, $[\mathbf{A}^s]_{if}$, gives the contribution of all the paths of length s steps from i to f to the effective rate constant. By adding up the contributions of the infinite number of paths connecting D to A, the following expression for $k_{\mathrm{A}\leftarrow\mathrm{D}}$ is obtained:[21]

$$k_{\mathrm{A}\leftarrow\mathrm{D}} = \sum_{i,f} k_{i\leftarrow\mathrm{D}} \frac{k_{\mathrm{A}\leftarrow f}}{\sum_q k_{q\leftarrow f}} \left(\sum_{s=1}^{+\infty} [\mathbf{A}^s]_{if}\right) \tag{50}$$

If the matrices of the eigenvectors ($\mathbf{R}$) and eigenvalues ($\mathbf{\Lambda}$) of $\mathbf{A}$ are introduced[21]

$$\mathbf{AR} = \mathbf{R\Lambda} \tag{51}$$

the matrix element $[\mathbf{A}^s]_{if}$ can be written as

$$[\mathbf{A}^s]_{if} = \sum_{q=1}^{N_{\mathrm{I}}} [\mathbf{R}]_{iq} [\mathbf{R}^{-1}]_{qf} \lambda_q^s \tag{52}$$

where λ_q is the qq element of the diagonal matrix $\mathbf{\Lambda}$, and the convergence value of the series in eq 50 can be calculated as[21]

$$\sum_{s=1}^{+\infty} [\mathbf{A}^s]_{if} = \sum_{q=1}^{N_{\mathrm{I}}} [\mathbf{R}]_{iq} [\mathbf{R}^{-1}]_{qf} \frac{\lambda_q}{1-\lambda_q} \tag{53}$$

dx.doi.org/10.1021/ct400690t | J. Chem. Theory Comput. 2013, 9, 5236−5246

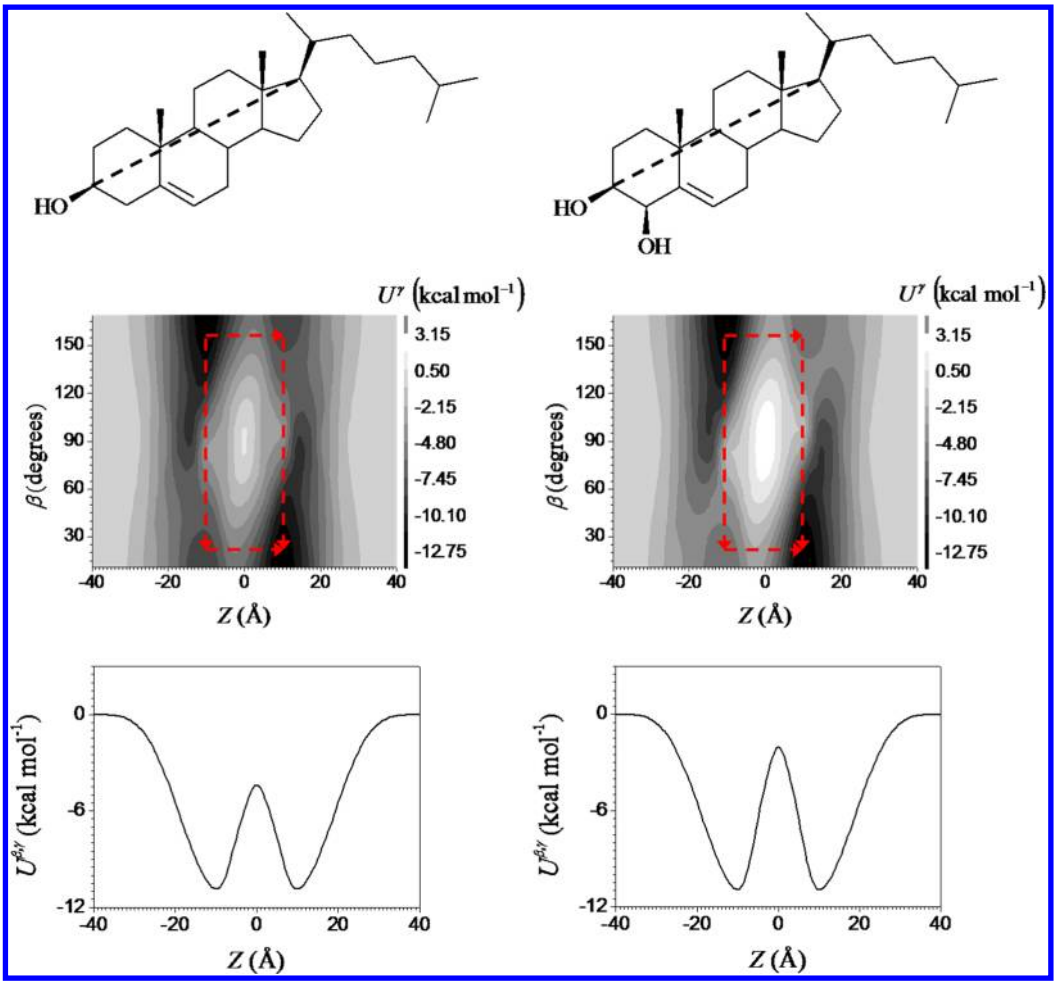

Figure 3. Molecular structure and free energy surface $U^{\gamma}(\beta,Z)$ and profile $U^{\beta,\gamma}(Z)$ calculated for **Chol** (left) and **4OH-Chol** (right) as a function of the distance Z of the molecular center of mobility from the bilayer midplane and of the angle β between the long molecular axis (shown on the molecular structure) and the bilayer normal. The arrows on the contour plots indicate the two flip-flop pathways that connect the absolute minimum in one leaflet with its equivalent in the other leaflet.

Substituting eqs 50 and 53 into eq 47 yields the expression for the permeability coefficient P in terms of the discrete transition rates:

$$P = l_D \sum_{i,f} k_{i\leftarrow D} \frac{k_{A\leftarrow f}}{\sum_q k_{q\leftarrow f}} \sum_{q=1}^{N_1} [\mathbf{R}]_{iq} [\mathbf{R}^{-1}]_{qf} \frac{\lambda_q}{1-\lambda_q} \quad (54)$$

RESULTS

A Case Study: The Permeability of Steroids. We will now focus on the permeability of steroids taken as illustrative examples and start by considering cholesterol (**Chol**) and 4-hydroxyl-cholesterol (**4OH-Chol**), in Figure 3. These are approximated as rigid molecules with nearly axial symmetry;[20,46] thus the relevant variables in the following analysis are Z, the steroid distance from the bilayer midplane, and β, the angle between the molecular long axis and the bilayer normal. The free energy landscapes, $U^{\gamma}(\beta,Z)$, that govern the diffusion process for the two molecules in a liquid crystalline DPPC bilayer at $T = 350$ K have been calculated using an implicit membrane model.[20,46] They are shown in Figure 3, where absolute and relative minima can be easily identified. In both cases, the height of the barriers beteween minima allows us to adopt a kinetic description.

In a previous study on cholesterol flip-flop, it was shown how transitions connecting the free energy minima can be given either a translational or an orientational character (Figure 3), and the relevance of the orientational transitions in the flip-flop kinetics, in particular, was assessed. In effect, the flip-flop rate was found to be determined by the inversion of the molecule from the upright to the upside-down orientation, taking place in the starting leaflet before the crossing of the bilayer midplane.[20] Thus, steroids seem to be suitable systems to investigate the role of roto-translational coupling on permeability.

In Table 1, we compare the flip-flop rate obtained for **Chol** and **4OH-Chol** from the two-dimensional (2D) analysis of the free energy surface $U^{\gamma}(\beta,Z)$ proposed in ref 20 with that calculated from a standard 1D approach. In the latter case, the rate constant is evaluated as the rate of escape from the minimum over the barrier in the free energy profile $U^{\beta,\gamma}(Z)$ obtained as the Boltzmann projection of the $U^{\gamma}(\beta,Z)$ surface on the positional coordinate (Figure 3). The approximate Kramers expression for the rate constant, which is the monodimensional analogue of eq 42, is used:

$$k_{\text{flip-flop}} = \frac{D_{\max}}{2\pi k_B T} \sqrt{|\ddot{U}^{\beta,\gamma}_{\max}| \ddot{U}^{\beta,\gamma}_{\min}} \exp\left[-\frac{U^{\beta,\gamma}_{\max} - U^{\beta,\gamma}_{\min}}{k_B T}\right] \quad (55)$$

where the free energy $U^{\beta,\gamma}$ and its curvature $\ddot{U}^{\beta,\gamma}$ in the minimum (min) and maximum (max) of the profile in Figure 3 appear, with the diffusion coefficient along the single coordinate of interest evaluated on the top of the barrier, $D_{\max}$.[22] The data reported in

dx.doi.org/10.1021/ct400690t | J. Chem. Theory Comput. 2013, 9, 5236−5246

Table 1 show that the 1D approach leads to an overestimation of the flip-flop rate, and the reason is that, as pointed out by the 2D analysis, the rate determining step of the process, which involves a reorientation, occurs along the β coordinate orthogonal to Z.[20]

Table 1. Flip-Flop Rate Constants Calculated for Chol and 4OH-Chol from the 2D Free Energy Surface[a,20] and from the 1D Free Energy Profile[22]

	2D	1D
Chol	2.0×10^4 s^{-1}	5.8×10^4 s^{-1}
4OH-Chol	4.8×10^2 s^{-1}	1.8×10^3 s^{-1}

[a]From the diffusion tensor calculated as explained in ref 20, an average translational diffusion coefficient equal to 1.3×10^{-6} cm^2 s^{-1} for **Chol** and **4OH-Chol** is calculated, which is used as D_{max} in eq 55.

The permeability coefficient for **Chol** and **4OH-Chol** can be calculated according to eq 54, in terms of the transitions shown in Figure 4. The symmetry of this system greatly simplifies the problem, and the resulting explicit expression can conveniently be written in the form:

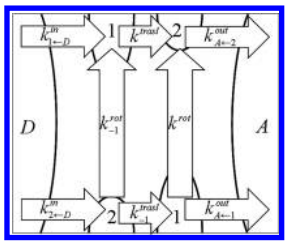

Figure 4. Schematic representation of the free energy surfaces shown in Figure 3, with transitions from donor D to acceptor A water basins and between the absolute 1 and relative 2 minima in the bilayer. Only half of the possible transitions are shown for symmetry reasons. In particular, the inverse of the $D \rightarrow 1,2$ transition coincides with the $1,2 \rightarrow A$ transition.

$$\frac{1}{P} = \frac{1}{2l_D}\left[\frac{k^{out}_{A\leftarrow 1}}{k^{in}_{1\leftarrow D}}\frac{1}{k^{trasl}} + \frac{(k^{in}_{1\leftarrow D} + k^{in}_{2\leftarrow D})\left(1 + 4\frac{k^{rot}}{k^{out}_{A\leftarrow 1}}\right) - 4k^{in}_{2\leftarrow D}\frac{k^{rot}}{k^{out}_{A\leftarrow 1}}}{k^{in}_{1\leftarrow D}\left((k^{in}_{1\leftarrow D} + k^{in}_{2\leftarrow D})\left(1 + \frac{k^{rot}}{k^{out}_{A\leftarrow 1}}\right) - k^{in}_{1\leftarrow D}\right)}\right] \quad (56)$$

where not all of the transition rates defined in Figure 4 enter, due to relations holding between them.

Equation 56 holds in general for free energy surfaces with the same features as those shown in Figure 3 and, depending on the specific characteristics of the system under investigation, can assume simpler forms. Crucial is the relative magnitude of k^{rot} and $k^{out}_{A\leftarrow 1}$.

In the limit $k^{rot} \ll k^{out}_{A\leftarrow 1}$, we can approximate

$$\frac{1}{P} \approx \frac{1}{2l_D}\left[\frac{k^{out}_{A\leftarrow 1}}{k^{in}_{1\leftarrow D}}\frac{1}{k^{trasl}} + \left(\frac{1}{k^{in}_{1\leftarrow D}} + \frac{1}{k^{in}_{2\leftarrow D}}\right)\right] \quad (57)$$

which is equivalent to the expression for the permeability coefficient in a system where rotational transitions are forbidden. This result can be seen as the sum of two independent contributions, brought by the two equivalent pathways represented in Figure 5A.

These are sequences of three steps, each associated with a resistance which is inversely proportional to the rate constant of the transition. As the intrinsic permeability P in the bilayer is defined with respect to bulk water, each resistance has to be rescaled for the free energy difference between the initial state of the transition and the water basins: hence, along the path at the top of Figure 5A, $1/k^{in}_{1\leftarrow D}$ remains unchanged, $1/k^{tr}$ is rescaled to $1/k^{out}_{A\leftarrow 1}/(1/k^{in}_{1\leftarrow D}k^{trasl})$, and $1/k^{out}_{A\leftarrow 2}$ to $k^{in}_{A\leftarrow 2}/(k^{in}_{2\leftarrow D}k^{out}_{A\leftarrow 2}) = 1/k^{in}_{2\leftarrow D}$ (see Figure 4). These step-associated resistances in series give the path-associated resistance (between brackets in eq 57). It can be shown that an analogous derivation along the path at the bottom of Figure 5A gives the same result. The combination of these two equivalent path-associated resistances in parallel yields the total resistance, that is, the inverse of the permeability coefficient in eq 57.

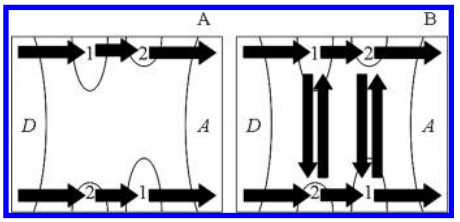

Figure 5. Sketch of permeation pathways allowed in limit cases with slow (A) or fast (B) rotational motions.

In the opposite case, when $k^{rot} \gg k^{out}_{A\leftarrow 1}$, we can write

$$\frac{1}{P} \approx \frac{1}{2l_D}\left[\frac{k^{out}_{A\leftarrow 1}}{k^{in}_{1\leftarrow D}}\frac{1}{k^{trasl}} + \frac{4}{k^{in}_{1\leftarrow D} + k^{in}_{2\leftarrow D}}\right] \quad (58)$$

which differs from eq 57 by a quantity that depends on the difference between $k^{in}_{1\leftarrow D}$ and $k^{in}_{2\leftarrow D}$.

Compared with the previous case, here, rotational transitions introduce alternative pathways: rapid rotations allow the system to preferentially follow those along which the resistance to permeation is the lowest, so increasing the overall permeability. The system behaves as if the stable states connected through rotational transitions were in equilibrium with one another, as illustrated in Figure 5B. Under these conditions, permeation can be treated as a monodimensional process along the single translational coordinate, having averaged out orientational effects, as in eq 36.

Both eqs 57 and 58 reduce to the same expression if $k^{in}_{1\leftarrow D} = k^{in}_{2\leftarrow D}$:

$$\frac{1}{P} = \frac{1}{2l_D}\left[\frac{k^{out}_{A\leftarrow 1}}{k^{in}_{1\leftarrow D}}\frac{1}{k^{trasl}} + \frac{2}{k^{in}_{1\leftarrow D}}\right] \quad (59)$$

It is worth noticing that none of eqs 57, 58, and 59 depend explicitly on rotational rate constants: the effect of the 2D dynamics on the permeation rate is rather enclosed in the 1/2 factor, which reflects the dimensionality of the process, and in the form of the second term in squared brackets, which represents the resistance to permeation that the solute encounters upon entering into and exiting from the lipid bilayer. The first term on the right-hand side of eqs 57, 58, and 59, which is preserved from the general expression in eq 56, represents the resistance arising from the diffusion of the solute through the inner region of the bilayer. Depending on the chemical nature of the solute, and hence on its affinity for the different regions of the membrane, one of the two contributions just illustrated can prevail.

From the height of the barriers in the free energy surfaces in Figure 3, which are reported in Table 2, it follows that $k^{rot} \gg k^{out}_{A\leftarrow 1}$

dx.doi.org/10.1021/ct400690t | J. Chem. Theory Comput. 2013, 9, 5236−5246

Table 2. Free Energy Barrier for Rotational ($(\Delta U^{\gamma})^{rot}$) and Exit ($(\Delta U^{\gamma})_{A\leftarrow 1}{}^{out}$) Transitions and Permeability Coefficients[a] Calculated for Chol, 4OH-Chol, and Dervatives without Tail

	$(\Delta U^{\gamma})^{rot}$ (kcal mol^{-1})	$(\Delta U^{\gamma})^{out}_{A\leftarrow 1}$ (kcal mol^{-1})	P (cm s^{-1})
Chol	6.3	12.7	4.7×10^{1}
4OH-Chol	8.1	12.7	4.7×10^{1}
Chol*	4.4	9.3	1.8×10^{1}
4OH-Chol*	5.8	9.2	5.0×10^{-1}

[a]Permeability coefficients were calculated using eq 36, with K^{Ω}_{eq} given by eq 60. D^{Ω}_{ZZeq} is taken equal to 1.3×10^{-6} cm^2 s^{-1} for **Chol** and **4OH-Chol** and equal to 1.6×10^{-6} for **Chol*** and **4OH-Chol*** in the center of the bilayer, equal to 4.4×10^{-6} cm^2 s^{-1} for **Chol** and **4OH-Chol** and equal to 5.2×10^{-6} for **Chol*** and **4OH-Chol*** at the water/bilayer interfaces. L = 40 Å is taken.

for both **Chol** and **4OH-Chol**. It may appear surprising that the permeation rate of these solutes is independent of the value of k^{rot}, which was shown to determine their flip-flop rate.[20] This is because, unlike in flip-flop, the reorientation is not the rate determining step of permeation. Instead, as clearly shown in Figure 6A by the profile of the average quantity entering eq 36:

$$\frac{1}{K^{\Omega}_{eq}(Z)} = \exp\left[\frac{U^{\beta,\gamma}(Z)}{k_B T}\right] \tag{60}$$

what limits the permeation rate of **Chol** and **4OH-Chol** is the crossing of the polar regions near the bilayer surfaces, which is represented by the second term in eq 58. Although the more polar derivative **4OH-Chol** shows a lower affinity than **Chol** for the hydrophobic region in the center of the bilayer (Figure 3), similar permeability coefficients are obtained for the two solutes, which are dominated by their unfavorable partitioning near the water/bilayer interfaces (Table 2). We could say that the lipid bilayer does not represent a barrier to the transport of these compounds whose diffusion is facilitated in the membrane with respect to bulk water by their high affinity for this environment.

But how general is this result? One could try to get out of the $k^{rot} \gg k^{out}_{A\leftarrow 1}$ limit by introducing polar substituents at the hydrophilic end of **Chol** molecule: this will enlarge the rotational barrier, thereby reducing k^{rot}, as observed for **4OH-Chol**, where however the effect is insufficient to change the behavior. On the other hand, for less hydrophobic solutes, characterized by shallower minima within the bilayer, $k^{out}_{A\leftarrow 1}$ will be larger. This is what occurs for derivatives of **Chol** and **4OH-Chol** lacking their hydrophobic tail (hereafter identified by ∗); in this case, however, k^{rot} also increases and remains much larger than $k^{out}_{A\leftarrow 1}$. The scarce affinity of **Chol*** for the central region of the bilayer with respect to bulk water, which is further reduced for **4OH-Chol*** by the presence of the additional hydroxyl group, makes their transport across this region more difficult than in the aqueous environment (Figure 6B,C). Thus, the weight of the first term in eq 58 is larger for **Chol*** than for **Chol** and **4OH-Chol** and even exceeds that of the second term for **4OH-Chol***. The same structural detail which distinguishes **Chol** and **4OH-Chol** without affecting their permeation rate produces a large difference between the permeability coefficients of **Chol*** and **4OH-Chol*** (Table 2), by influencing their partitioning in the most critical region for permeation.

CONCLUSIONS

The monodimensional description of solute permeability through lipid bilayers proposed in the inhomogeneous solubility-diffusion model has been recently questioned: besides the translational coordinate, which represents the displacement of the solute along the bilayer normal, a possible role of other degrees of freedom in the translocation process has been claimed. Here, we have focused on the orientational coordinates, which have been included in a general formalism based on the roto-translational Fokker−Planck equation. We have shown that, under the conditions where this can be reduced to a kinetic description, the permeability coefficient can be expressed as the sum of the contributions of all possible pathways connecting the donor and acceptor basins at the two sides of the membrane. This approach has been applied to steroid molecules, which have been taken as a case study: based on the free energy surface governing their diffusion across the bilayer, we have obtained a simple form of the permeability coefficient in terms of the rate constants for the rotational and translational transitions. Steroid derivatives differing in the number of hydroxyl groups at their polar end, and in the presence of the alkyl tail at the opposite one, have been considered. Two kinds of behavior have been distinguished. The permeation rate of long derivatives is controlled by diffusion near the bilayer surfaces and is essentially independent of molecular details, which determine what occurs in the interior of the bilayer. The lower affinity of short derivatives for the bilayer environment causes the rising of the barrier associated with diffusion near the

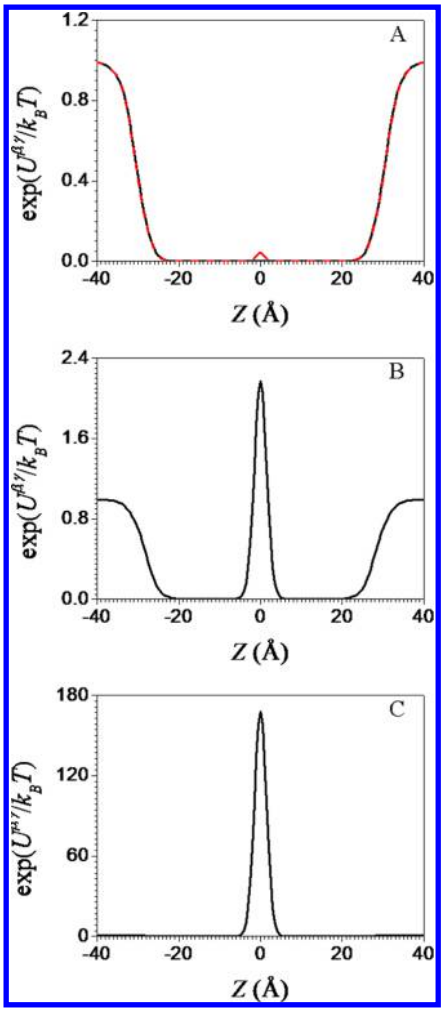

Figure 6. $1/K^{\Omega}_{eq}(Z)$ profiles (eq 60) calculated for **Chol** (A, black solid line) and **4OH-Chol** (A, red dashed line), **Chol*** (B), and **4OH-Chol*** (C).

dx.doi.org/10.1021/ct400690t | J. Chem. Theory Comput. 2013, 9, 5236−5246

center of the bilayer, so their permeability is determined by the crossing of this barrier, whose height is sensitive to molecular polarity. In none of these cases is the permeation rate determined by molecular reorientations, which was shown to be critical for the flip-flop rate: the role of rotational motion is simply that of averaging the orientational effects, so that a monodimensional description can capture the relevant aspects of the permeation process. What we have found for steroid derivatives is likely to be a general behavior which justifies the use of the standard solubility-diffusion model for relatively small and rigid molecular solutes.

APPENDIX A

Explicit Form of $\vec{\nabla}$ and D

The explicit form of $\vec{\nabla}$ in the laboratory frame LF is given by

$$\vec{\nabla} = \begin{pmatrix} \vec{\nabla}_{\text{transl}} \\ \vec{\nabla}_{\text{rot}} \end{pmatrix}; \ \vec{\nabla}_{\text{transl}} = \begin{pmatrix} \frac{\partial}{\partial X} \\ \frac{\partial}{\partial Y} \\ \frac{\partial}{\partial Z} \end{pmatrix} \ \vec{\nabla}_{\text{rot}} = \begin{pmatrix} \frac{\partial}{\partial \alpha} \\ \frac{\partial}{\partial \beta} \\ \frac{\partial}{\partial \gamma} \end{pmatrix} \tag{A1}$$

In the absence of dynamic roto-translational coupling, the diffusion tensor $\mathbf{D}$ expressed in the *LF* has the form:[42]

$$\mathbf{D}(\Omega, Z) = \begin{pmatrix} \mathbf{D}_{\text{transl}}(\Omega, Z) & 0 \\ 0 & \mathbf{D}_{\text{rot}}(\Omega, Z) \end{pmatrix}$$

$$\mathbf{D}_{\text{transl}} = \begin{pmatrix} D_{XX} & D_{XY} & D_{XZ} \\ D_{YX} & D_{YY} & D_{YZ} \\ D_{ZX} & D_{ZY} & D_{ZZ} \end{pmatrix} \ \mathbf{D}_{\text{rot}} = \begin{pmatrix} D_{\alpha\alpha} & D_{\alpha\beta} & D_{\alpha\gamma} \\ D_{\beta\alpha} & D_{\beta\beta} & D_{\beta\gamma} \\ D_{\gamma\alpha} & D_{\gamma\beta} & D_{\gamma\gamma} \end{pmatrix} \tag{A2}$$

The transformations relating the diffusion tensors in eq A1, defined in LF, to the Cartesian tensors $\mathbf{D}^{\text{MF}}_{\text{transl}}$ and $\mathbf{D}^{\text{MF}}_{\text{rot}}$, defined in the molecular frame MF, are given by[42]

$$\mathbf{D}^{\text{LF}}_{\text{transl}}(\Omega, Z) = \mathbf{R}^{T}(\Omega)\mathbf{D}^{\text{MF}}_{\text{transl}}(\Omega, Z)\mathbf{R}(\Omega)$$

$$\mathbf{D}_{\text{transl}}(\Omega, Z) = \mathbf{D}^{\text{LF}}_{\text{transl}}(\Omega, Z) \tag{A3}$$

with

$$\mathbf{R}(\Omega) = \begin{pmatrix} \cos\beta\cos\gamma & \sin\gamma & -\sin\beta\cos\gamma \\ -\cos\beta\sin\gamma & \cos\gamma & \sin\beta\sin\gamma \\ \sin\beta & 0 & \cos\beta \end{pmatrix} \tag{A4}$$

and

$$\mathbf{D}^{\text{LF}}_{\text{rot}}(\Omega, Z) = \mathbf{R}^{T}(\Omega)\mathbf{D}^{\text{MF}}_{\text{rot}}(\Omega, Z)\mathbf{R}(\Omega)$$

$$\mathbf{D}_{\text{rot}}(\Omega, Z) = \mathbf{M}(\Omega)\mathbf{D}^{\text{LF}}_{\text{rot}}(\Omega, Z)\mathbf{M}^{T}(\Omega) \tag{A5}$$

with

$$\mathbf{M}(\Omega) = \begin{pmatrix} -\cos\beta/\sin\beta & 0 & 1 \\ 0 & 1 & 0 \\ 1/\sin\beta & 0 & 0 \end{pmatrix} \tag{A6}$$

AUTHOR INFORMATION

Corresponding Author

*E-mail: giulia.parisio@unipd.it. Phone: +39 049 8275245.

Author Contributions

The manuscript was written through contributions of all authors. All authors have given approval to the final version of the manuscript.

Notes

The authors declare no competing financial interest.

ACKNOWLEDGMENTS

This work was supported by the Università degli Studi di Padova (PRAT 2009 and Junior Grant 2011).

ABBREVIATIONS

DOPC, 1,2-oleoyl-*sn*-glycero-3-phosphocholine; DPPC, 1,2-dipalmitoyl-*sn*-glycero-3-phosphocholine; DPS, discrete path sampling; MD, molecular dynamics; POPC, 1-palmitoyl-2-oleoyl -*sn*-glycero-3-phosphocholine

REFERENCES

(1) Sugano, K.; Kansy, M.; Artursson, P.; Avdeef, A.; Bendels, S.; Di, L.; Ecker, G. F.; Faller, B.; Fischer, H.; Gerebtzoff, G.; Lennernaes, H.; Senner, F. *Nat. Rev.* **2010**, *9*, 597−614.
(2) Missner, A.; Pohl, P. *ChemPhysChem* **2009**, *10*, 1405−1414.
(3) Avdeef, A.; Artursson, P.; Neuhoff, S.; Lazorova, L.; Gråsjö, J.; Tavelin, S. *Eur. J. Pharm. Sci.* **2005**, *24*, 333−349.
(4) Mansy, S. S. *Cold Spring Harbor Perspect. Biol.* **2010**, *2*, a002188:1−14.
(5) Overton, C. E. *Vierteljahrsschr. Naturforsch. Ges. Zuerich* **1899**, *44*, 88−135.
(6) Kleinzeller, A. *Curr. Top. Membr.* **1999**, *48*, 1−22.
(7) Liu, X.; Testa, B.; Fahr, A. *Pharm. Res.* **2010**, *28*, 962−977.
(8) Finkelstein, A. *J. Gen. Physiol.* **1976**, *68*, 127−135.
(9) Lieb, W. R.; Stein, W. D. *Curr. Top. Membr. Transp.* **1971**, *2*, 1−39.
(10) Walter, A.; Gutknecht, J. *J. Membr. Biol.* **1986**, *90*, 201−217.
(11) Xiang, T.-X.; Chen, X.; Anderson, B. D. *Biophys. J.* **1992**, *63*, 78−88.
(12) Xiang, T.-X.; Xu, Y.-H.; Anderson, B. D. *J. Membr. Biol.* **1998**, *165*, 77−90.
(13) Xiang, T.-X.; Anderson, B. D. *J. Membr. Biol.* **1994**, *140*, 111−122.
(14) Xiang, T.-X.; Anderson, B. D. *Biophys. J.* **1998**, *75*, 2658−2671.
(15) De Young, L. R.; Dill, K. A. *J. Phys. Chem.* **1990**, *94*, 801−809.
(16) Nagle, J. F.; Mathai, J. C.; Zeidel, M. L.; Tristram-Nagle, S. *J. Gen. Physiol.* **2008**, *131*, 77−85.
(17) Diamond, J. M.; Katz, Y. *J. Membr. Biol.* **1974**, *17*, 121−154. Diamond, J. M.; Szabo, G.; Katz, Y. *J. Membr. Biol.* **1974**, *17*, 148−152.
(18) Marrink, S.-J.; Berendsen, H. J. C. *J. Phys. Chem.* **1994**, *98*, 4155−4168.
(19) Orsi, M.; Essex, J. W. In *Molecular simulations and Biomembranes: from Biophysics to Function*; Biggin, P. C., Sansom, M. S. P., Eds.; Royal Society of Chemistry: London, 2010; pp 77−91.
(20) Parisio, G.; Sperotto, M. M.; Ferrarini, A. *J. Am. Chem. Soc.* **2012**, *134*, 12198−12208.
(21) Wales, D. J. *Mol. Phys.* **2002**, *100*, 3285−3305.
(22) Kramers, H. A. *Physica* **1940**, *7*, 284−304.
(23) Ulander, J.; Haymet, A. D. J. *Biophys. J.* **2003**, *85*, 3475−3484.
(24) Orsi, M.; Essex, J. W. *Soft Matter* **2010**, *6*, 3797−3808.
(25) Marrink, S.-J.; Berendsen, H. J. C. *J. Phys. Chem.* **1996**, *100*, 16729−16738.
(26) Bemporad, D.; Essex, J. W.; Luttmann, C. *J. Phys. Chem. B* **2004**, *108*, 4875−4884.
(27) Xiang, T.-X.; Anderson, B. D. *Adv. Drug Delivery Rev.* **2006**, *58*, 1357−1378.
(28) Swift, R. V.; Amaro, R. E. *Chem. Biol. Drug Des.* **2013**, *81*, 61−71.

(29) Leung, S. S.; Mijalkovic, J.; Borrelli, K.; Jacobson, M. P. *J. Chem. Inf. Model.* **2012**, *56*, 1621−1636.
(30) Berezhkovskii, A.; Szabo, A. *J. Chem. Phys.* **2005**, *122*, 014583:1−4.
(31) Neale, C.; Bennett, W. F. D.; Tieleman, D. P.; Pomès, R. *J. Chem. Theory Comput.* **2011**, *7*, 4175−4188.
(32) Cardenas, A. E.; Jas, G. S.; DeLeon, K. Y.; Hegefeld, W. A.; Kuczera, K.; Elber, R. *J. Phys. Chem. B* **2012**, *116*, 2739−2750.
(33) Ghaemi, Z.; Minozzi, M.; Carloni, P.; Laio, A. *J. Phys. Chem. B* **2012**, *116*, 8714−8721.
(34) Jämbeck, J. P. M.; Lyubartsev, A. P. *J. Phys. Chem. Lett.* **2013**, *4*, 1781−1787.
(35) Kampf, J. P.; Kleinfeld, A. M. *Physiology* **2007**, *22*, 7−29.
(36) Kessel, A.; Musafia, B.; Ben-Tal, N. *Biophys. J.* **2001**, *80*, 2536−2545.
(37) Oren, I.; Fleishman, S. J.; Kessel, A.; Ben-Tal, N. *Biophys. J.* **2004**, *87*, 768−779.
(38) Vivcharuk, V.; Kaznessis, Y. N. *J. Phys. Chem. B* **2011**, *115*, 14704−14712.
(39) Rose, M. E. *Elementary Theory of Angular Momentum*; John Wiley & Sons: New York, 1957.
(40) Risken, H. The Fokker-Planck equation. *Methods for Solution and Applications*, 2nd ed.; Springer-Verlag: Berlin, 1989.
(41) Gardiner, C. W. Handbook of Stochastic Methods. *For Physics, Chemistry and the Natural Sciences*, 2nd ed.; Springer-Verlag: Berlin, 1985.
(42) Frezzato, D.; Polimeno, A.; Ferrarini, A.; Moro, G. J. *Theor. Chem. Acc.* **2007**, *117*, 1017−1027.
(43) Moro, G. J.; Ferrarini, A.; Polimeno, A.; Nordio, P. L. In *Reactive and Flexible Molecules in Liquids*; Dorfmuller, T., Ed.; Kluwer Academic Publishers: Dordrecht, The Netherlands, 1989; pp 107−139.
(44) Van Kampen, N. G. *Stochastic Processes in Physics and Chemistry*, 3rd ed.; Elsevier: Amsterdam, The Netherlands, 2007.
(45) Langer, J. S. *Ann. Phys.* **1969**, *54*, 258−275.
(46) Parisio, G.; Ferrarini, A. *J. Chem. Theory Comput.* **2010**, *6*, 2267−2280.